ANNUAL REVIEWS

Annual Review of Physical Chemistry

Modeling Anharmonic Effects in the Vibrational Spectra of High-Frequency Modes

Edwin L. Sibert III

Department of Chemistry and Theoretical Chemistry Institute, University of Wisconsin–Madison, Madison, Wisconsin, USA; email: elsibert@wisc.edu

Annu. Rev. Phys. Chem. 2023. 74:219–44

First published as a Review in Advance on January 25, 2023

The *Annual Review of Physical Chemistry* is online at physchem.annualreviews.org

https://doi.org/10.1146/annurev-physchem-062422-021306

Keywords

vibrations, mode mixing, anharmonicities, resonances

Abstract

High-resolution vibrational spectra of C–H, O–H, and N–H stretches depend on both molecular conformation and environment as well as provide a window into the frequencies of many other vibrational degrees of freedom as a result of mode mixing. We review current theoretical strategies that are being deployed to both aid and guide the analysis of the data that are encoded in these spectra. The goal is to enhance the power of vibrational spectroscopy as a tool for probing conformational preferences, hydrogen bonding effects away from equilibrium, and energy flow pathways. Recent years have seen an explosion of new methods and strategies for solving the nuclear Schrödinger equation. Rather than attempt a comprehensive review, this work highlights specific molecular systems that we have chosen as representing bonding motifs that are important to chemistry and biology. We focus on the choices theoretical chemists make regarding the level of electronic structure theory, the representation of the potential energy surface, the selection of coordinates, preferences in basis sets, and methods of solution.

1. INTRODUCTION

This review examines theoretical approaches to interpreting the intriguing spectral features associated with C–H, O–H, and N–H stretch molecular vibrations. Rather than observing a single transition for each of these vibrations, there are many transitions whose presence is a result of resonance interactions with other energetically near-lying states. The rich information content embedded in the numbers, positions, and intensities of these lines allows scientists to gain insights into motions of molecules and the features of the potential energy landscapes that lead to these motions. In so doing, they learn about hydrogen bonding strengths, conformational preferences, and energy flow pathways. The information content of IR and Raman spectra is most clearly revealed with theoretical calculations supporting innovative experiments, and this review focuses on such comparisons. Rather than explore one technique or a specific molecular system, we review select works in this field that enable us to highlight common threads of research. In exploring the similar approaches to complex problems, one can get a better understanding of the underlying challenges to the theoretical modeling of high-frequency vibrations.

This area of research is backed by an ever advancing and growing theoretical machinery comprised of powerful computers and elegant computational algorithms. The goal of all this research is to solve the nuclear time-independent Schrödinger equation (TISE) and interpret the results. There are three crucial steps in the solution process. First, one must express the Hamiltonian and dipole moments as functions of their coordinates and for the former the conjugate momenta. Second, one must choose a representation or basis so that one can express the Hamiltonian in a matrix form. Finally, one must be able to find the associated eigenvalues, eigenfunctions, and intensities for the $3N - 6$ degree of freedom Hamiltonian, where N is the number of atoms. There is a continuum of variations and extensions to each of these steps, and the methods one pursues in calculating these quantities depend on the size of the system and how accurately one wants to know a select set of these eigenfunctions, eigenvalues, and intensities. The approach one prefers depends sensitively on the scientific questions one is trying to answer and the research interests and skills of the investigator.

Although kinetic energy operators can be complex, the biggest challenge to expressing a Hamiltonian as a function of positions and momenta is the potential energy, and perhaps its derivatives, at select configurations of the atoms that make up the molecular system. Electronic structure packages enable one to do this. One chooses the appropriate level of calculation based on computer resources and accuracy, accepting the fact that the desired accuracy is often unattainable given one's resources. Having calculated the potential at select points one determines the potential energy surface (PES) that describes the functional dependence of the potential in a form that allows for easy evaluation at arbitrary points (1–13). A common goal is to find the best global representation using the fewest ab initio points. The resulting expressions need to be rewritten in a set of coordinates and in a form that allows for easy evaluation of matrix elements. These coordinates should also minimize the kinetic couplings and allow for ready evaluation of those matrix elements. In making these choices, one must do so with a basis set in mind. A notable example is the basis of discrete variable representations (DVRs) for which the potential matrix integrals reduce to evaluating the potential at select points in configuration space (14).

The final step, as mentioned above, is to solve for the eigenvalues and intensities. Direct matrix diagonalization is the most straightforward approach. Unfortunately, the computation time for this method scales as N^3, where N is the size of the basis set. For this reason, there are important algorithmic advances occurring that are extending the size of molecules and values of energies that can be treated by exploiting iterative methods. In instances in which memory storage becomes an issue, matrix iteration methods such as those by Lanczos (15–21) and Davidson

(22) have proven more useful than those of direct diagonalization. These methods rely on rapid matrix product evaluations that are aided by efficient storage. Garnier clearly delineates many of the central advances in this area (23). Basis set contractions have long been a pivotal way to reduce the size of variational calculations and costs of storing wave functions. Recently, however, workers have turned to the methods of tensorial factorization as a powerful technique for achieving similar goals (24–30). The alternating least squares minimization approach (31) is one of the most popular ways of carrying out this factorization.

Excellent packages have been developed that take advantage of the abovementioned considerations. These include TROVE (32), MULTIMODE (33, 34), GENIUSH (35, 36), DYNAMOL (37), and PyVCI (38, 39), as well as those based on the multiconfiguration time-dependent Hartree (MCTDH) method (40–43). The variety of systems and the coupling pathways that are encountered in molecular systems benefit from different sets of approximations, representations, and ease of interpretation. Each of the above software packages has areas in which they excel.

Against this backdrop, our work examines a selection of systems of experimental interest. Given the breadth of the field, the review highlights specific problems in which including anharmonicities and mode mixing is essential. We begin with normal modes, as they are both the simplest and most important tool for describing vibrations. We then consider perturbative treatments that highlight the importance of resonances as well as electrical and mechanical anharmonicities. Closely related to perturbative treatments are effective Hamiltonian treatments in which simple local mode Hamiltonians are used to describe how the C–H stretch region can be used to distinguish conformational preferences, even though this is a region dominated with Fermi coupling interactions with scissor modes. Our review then turns to reduced-dimensional treatments of ab initio–based Hamiltonians. For O–H and N–H stretches, we review studies of bonding motifs that are chosen to gain insights into hydrogen-bonding effects that are realized as a result of molecular motions. In the final part of our review, we examine three very different treatments of the vibrations of the formic acid molecule focusing on the factors mentioned above, and we place them within the context of current research activities to assign spectra and interpret resonance couplings. This component of the review highlights the techniques used to represent the potential and to solve the nuclear TISE. We choose this molecule because the extensive spectroscopic data that are available provide an excellent benchmark for describing the coupling pathways due to the many resonance interactions. As such, the analysis provides a challenge to perturbative techniques that are currently receiving substantial interest. In addition, the molecule has a low-energy conformer that requires potential fitting strategies beyond the typical Taylor series expansion of normal modes.

2. HIGH-RESOLUTION SINGLE-CONFORMER SPECTROSCOPY AIDED BY NORMAL MODES

For many molecular studies, especially those of semirigid molecules, normal mode investigations of the lower-frequency modes provide the desired level of theory for determining spectral assignments and conformational preferences. Given their importance, we review such treatments before moving on to our treatments of anharmonicities.

High-resolution single-conformer vibrational spectroscopies (44–51) of large biomolecules allow experimentalists to uncover spectral patterns that are hidden at room temperatures. Normal mode calculations have proven to be critically important in modeling the observed line positions and intensities in order to identify bonding preferences. These calculations are carried out with electronic structure computer packages that provide stable structures and IR spectral positions based on the double harmonic approximation. The force field is assumed to be harmonic, and the dipoles are approximated as having constant and linear contributions. The most widely

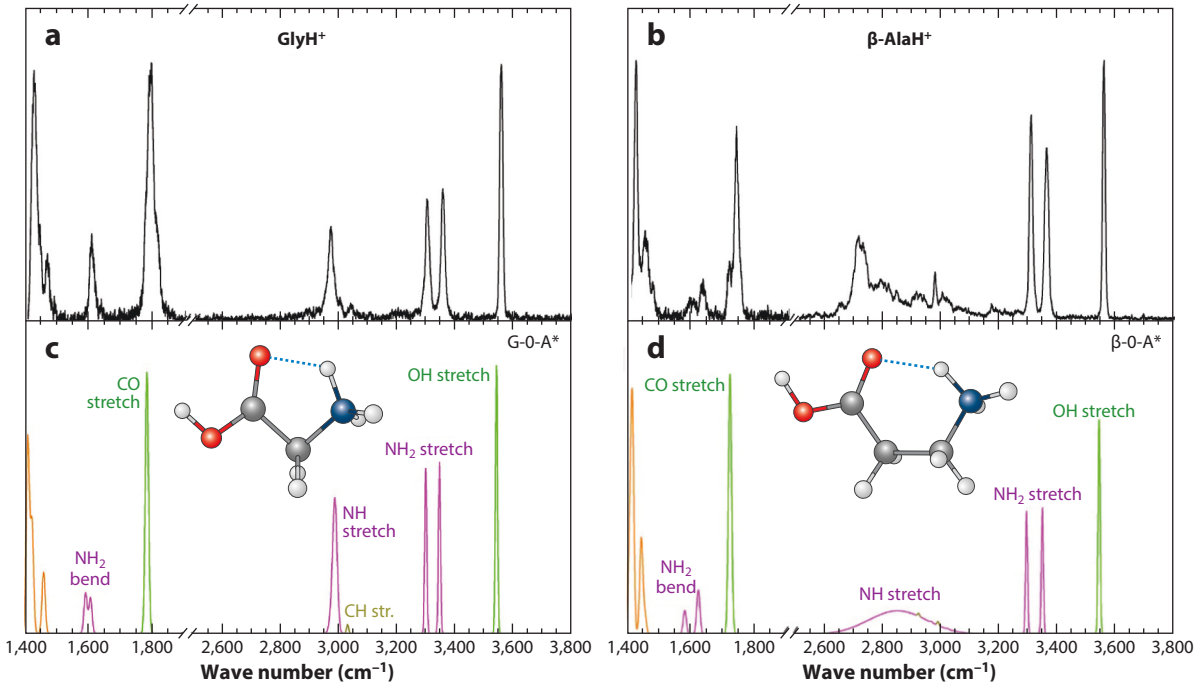

Figure 1

IR predissociation spectra of $GlyH^+(D_2)$ (*a*) and β-$AlaH^+(D_2)$ (*b*) compared with harmonic spectra calculated at the cam-B3LYP (*c*) and def2TZVP/GD3BJ (*d*) levels. An asterisk indicates an isomer that has been assigned to the experimental spectrum. The spectra cover the frequency range, from NH_2 bends to OH stretches. Figure adapted with permission from Reference 53; copyright 2020 American Chemical Society.

used theories are scaled density functional methods that have the advantage of being fast and reasonably accurate (52). Andersson & Uvdal (52) found a scaling for the B3LYP/6-311+G(d,p) basis that leads to agreement of 93% of the fundamentals being predicted to within 2% of the experimental results for a large data set.

The work of Fischer et al. (53) provides a nice example of this approach. They recorded high-resolution D_2-tagged IR spectra of the $GlyH^+(H_2O)_n$ and β-$AlaH^+(H_2O)_n$ species in order to reveal and compare the microsolvation motifs. **Figure 1** shows a comparison between normal mode theory and a D_2-tagged IR spectrum of the bare species. This study includes additional comparisons of the successively hydrated species that allow their bonding preferences to be determined. The study of such clusters is significant; these relatively small systems offer a spectral resolution, as is evident in **Figure 1**, that allows us to test our ability to predict the relative stability conformers, a stability that depends sensitively on the same noncovalent interactions and hydrogen bonding strengths as those found in the liquid phase.

A second example of the power of the scaled density functional theory (DFT) approach is evident in the study of Lawler et al. (54). The goal there was to reveal conformational preferences of peptide backbone structures that were designed to form β-hairpin loops. The single scaling factor that is typically used was found to be inadequate for the 1,600–1,800 cm^{-1} region, a region that is commonly associated with the amide I vibrations. In these protonated peptides the C=O stretch fundamentals can experience extensive mixing with the N–H bending fundamentals of the NH_3^+ group. A scaled localized normal mode Hamiltonian was developed that has one scaling

factor for C=O stretches and another for the N–H bending. This updated model describes this spectral region with enough accuracy to allow the conformer specific spectra to be assigned to computationally determined low-energy structures.

3. APPLICATIONS OF SECOND-ORDER PERTURBATION THEORY

3.1. General Implementation Considerations

To improve on normal mode predictions of transition energies and intensities, one needs to include anharmonicities and higher levels of electronic structure theory. A simple and time-honored approach for doing this is to calculate the cubic and select quartic terms in the Taylor series expansion of the potential with respect to the normal modes for use in second-order perturbation theory (55, 56), although local modes have also been found to be effective for perturbative treatments (57–59). The normal coordinate Taylor series expansion coefficients are readily calculated using finite differences of Hessian elements that can be calculated analytically with many levels of electronic structure theory. These methods have been incorporated into many electronic structure packages for use in what is now referred to as vibrational second-order perturbation theory (VPT2).

The VPT2 level of treatment of the vibrations has been shown to be sufficiently accurate that one can use it to test the quality of PESs. A study that clearly demonstrates this is the Puzzarini et al. (60) investigation of the vibrations of uracil. An important aspect of this work is that the authors build on the idea of Handy and coworkers (61) to demonstrate the utility of hybrid methods in the force field description. Hybrid methods are widely used and involve calculating quadratic terms at a higher level of theory than the cubic and quartic terms. The motivation is clear. There are far fewer quadratic terms than cubic and quartic terms, the spectral results are most sensitive to the quadratic terms, and the higher-order terms are less sensitive to the level of electronic structure theory. Puzzarini et al. (60) explored the use of coupled-cluster level theory for energies and intensities with and without anharmonic terms calculated at the density functional level. This study compares hybrid results to MP2-level calculations, focusing on the role of basis sets as well as the perturbative treatment of the resonant coupling terms.

In a systematic and wide-ranging investigation, Roy et al. (62) and more recently Roy (63) have compared the energies and intensities of fundamentals and overtones that have been calculated with second-order perturbation theory using a zero-order vibrational self-consistent field (VSCF) basis for results of various levels of electronic structure theory. Roy and colleagues found that the CCSD(T)/cc-pVTZ basis yields a 1.4% mean absolute error for the 135 fundamentals of 16 molecules.

3.2. VPT2 Applications

VPT2 can be used to model the O–H and C–H stretching regimes if one is thoughtful in the treatment of the Fermi resonance interactions (64–71). The recent work by Lee and coworkers on IR spectroscopy of polycyclic aromatic hydrocarbons (PAHs) should be mentioned in this regard (64–66). Owing to the many resonance interactions, a large polyad model (72) is constructed, allowing for many interacting states. These studies were based on DFT force fields due to the large size of the PAH molecules. The resonance identification was based on separate force constant magnitudes and energy difference thresholds. The quality of their C–H stretching predictions was impressive given the wide range of PAH sizes that were considered. Interestingly, for some of the larger PAHs (73), the experimental spectra are more congested than the theoretical predictions. Given our current understanding of the onset of state mixing in large

systems (74), it is not surprising that simple polyad treatments of C–H stretches are not able to describe eigenstate-resolved spectra in large molecules.

Looking at smaller systems, Franke et al. (70) applied VPT2 to the study of *i*-propyl and *n*-propyl with good success. The C–H stretch regime of these radicals was measured by generating the radicals in the gas phase and promptly solvating them in a beam of He nanodroplets. This work was followed by an in-depth perturbative analysis of which anharmonic terms should be treated as resonances in the C–H stretch regions for several molecules (71). **Figure 2** shows the impressive results from that work (71), in which different predicted spectra correspond to the different criteria that were considered in **Figure 2*a–d*** for identifying interactions as being resonant.

This work also carefully describes the importance of choosing the appropriate levels of theory and basis sets in the electronic structure calculations. In the comparison shown in **Figure 2**, the potential was calculated at the CCSD(T) level of theory using atomic natural orbital basis states (75), a basis that appears to provide exceptional results. As is commonly done, the force field is a hybrid force field in which the quadratic couplings are calculated with an ANO1 basis set and the cubic/quartic and dipole terms are calculated with ANO0 basis sets. To appreciate the quality of this work, the reader should compare the scale of the wave number axes in **Figures 1** and **2**.

Electrical anharmonicity is caused by higher-order terms in the dipole moment expansion. Given the similarity between **Figure 2*d*** and **Figure 2*e***, one might conclude that electrical anharmonicity is relatively unimportant for describing this spectral region. We now turn to a system in which this is definitely not the case.

Stropoli et al. (67, 68), in an experimental/theoretical collaboration, have recorded the spectra of H_2-tagged cryogenically cooled $X^- \cdot HOCl$ (X = Cl, Br, and I) ion–molecule complexes (see **Figure 3**) with the goal of examining the spectroscopic implications of a strong anionic H-bond to an acid OH group. The work builds on previous studies of the less acidic $X^- \cdot HOH$ ion complex. Spectra in both the O–H stretching and HOCl bending regimes were recorded to examine the effects of varying acidity. A beautiful feature of this system is that as the acidity increases from X = I to Cl, the O–H stretch frequency decreases and is essentially tuned through a Fermi resonant interaction with the OH bend overtone, with $Br^- \cdot HOCl$ showing the most pronounced resonant coupling. This simple resonant picture, however, cannot alone account for the spectral complexity, and theoretical calculations were needed to discover the nature of the coupling mechanisms.

VPT2 was carried out with the PyVibPTn package (69) to investigate the coupling using MP2/aug-cc-pVTZ levels of theory for X = Cl and Br and MP2/aug-cc-pVTZ-pp and effective core potentials for X = I. This code allows both excitation of states with more than two quanta and substantial flexibility in the choice of resonances. As in the work of Franke et al. (71), and as demonstrated in **Figure 2**, this flexibility is crucial when investigating states with complicated coupling pathways. A surprising finding was that there are low-frequency modes between the ion and the complex that reveal themselves as important contributors to the richness of the spectral congestion.

Even at the frequency of the OH bend there are several surprising features that are revealed. The double-harmonic approximation predicts a single line corresponding to excitation of the bend fundamental. However, as can be seen in **Figure 4**, there are additional peaks. The expected ν_{HOCl} transitions are shown for both the VPT2 theory and the experiment. The theoretical analysis revealed that the out-of-plane H motion has a large quadratic dipole moment that arises owing to this motion, modulating the strength of the H-bonding interaction. This effect is so pronounced that it leads to the overtone $2\nu_{oop_H}$ having an oscillator strength that is often larger than the bend fundamental. Furthermore, moving from right to left in the figure corresponds to increasing the basicity of X^-, and one clearly sees the corresponding shift of the overtone to higher

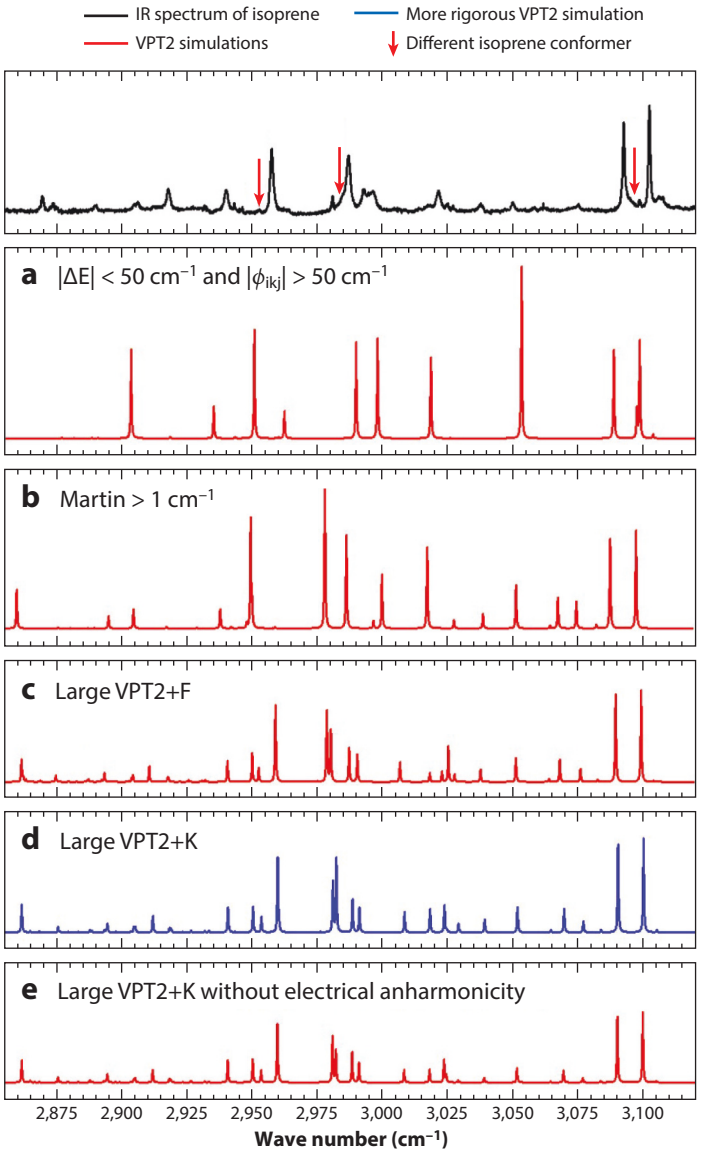

Figure 2

IR spectrum of isoprene compared with various VPT2 simulations. The most rigorous simulation is shown in blue. (*a*) VPT2+F based on individual energy difference and force constant magnitude tests. (*b*) VPT2+F based on the Martin test. (*c*) VPT2+F based on the "large effective Hamiltonian" model. (*d*) VPT2+K based on the "large effective Hamiltonian" model. (*e*) VPT2+K based on the "large effective Hamiltonian" model and assuming electrical harmonicity. Transitions due to a different isoprene conformer are indicated with arrows. Figure adapted with permission from Reference 71; copyright 2021 American Chemical Society. Abbreviation: VPT2, vibrational second-order perturbation theory.

wave numbers. Intriguingly, for the intermediate case shown in **Figure 4*b*** the second line vanishes. The authors explain this disappearance as a result of destructive interference of two bright states that have mixed because they are Fermi coupled, a result that is revealed in the VPT2 calculations.

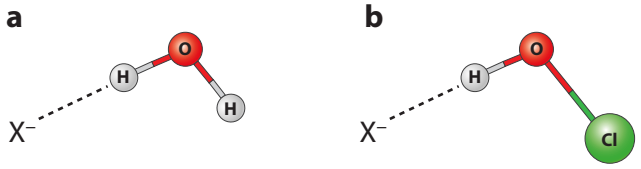

Figure 3

Comparison of hydrogen bonding modifications in (*a*) $X^- \cdot HOH$ and (*b*) $X^- \cdot HOCl$. Figure adapted from Reference 67 with the permission of AIP Publishing.

4. EFFECTIVE HAMILTONIANS FOR C–H STRETCHES

The Zwier group has pioneered the use of resonant ion–dip IR (RIDIR), fluorescence-dip IR (FDIR), and UV–UV hole burning spectroscopies to probe molecules in supersonic expansions to record conformer-specific spectra (44, 45). Using the results of these methods, the Zwier and Sibert groups have collaborated to develop effective Hamiltonians for the C–H stretch region of the IR spectra (76–80). The form of these Hamiltonians is based on second-order perturbation theory. In contrast to the above VPT2 descriptions, they chose to work in a set of localized normal modes (79, 81–83). The Reiher group (84, 85) realized, whenever a molecule has a number of characteristic vibrations consisting of close-lying delocalized normal modes, that one can carry out an orthogonal transformation of the corresponding normal coordinates and obtain a new set of modes that describe spatially localized vibrations. Different schemes have been proposed for carrying out the localization (76, 84–89), but we have found, that for C–H stretches and CH_2 scissors, the results are insensitive to the details of the localization scheme. The starting point of our approach is a Hessian calculated at the B3LYP/6-311++(d,p) level of theory. Using cyclohexane as an example (90), diagonalization of the Hessian yields six normal modes that correspond to scissor vibrations. The appropriate orthogonal transformation of these modes leads to the localized scissor modes.

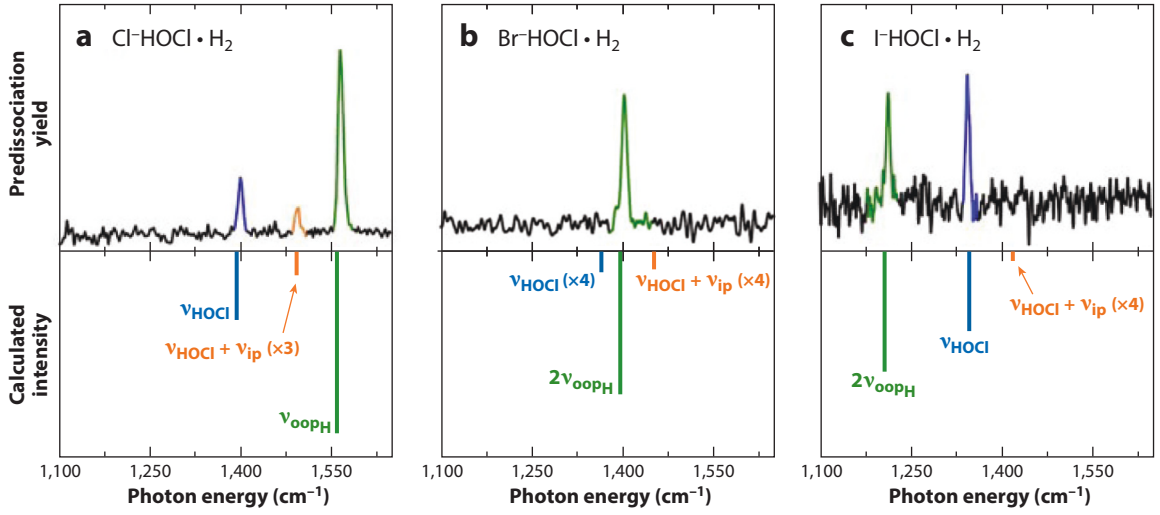

Figure 4

H_2-tagged $X^- \cdot HOCl$ spectra for (*a*) X = Cl, (*b*) X = Br, and (*c*) X = I are compared with inverted stick spectra calculated at the MP2/aug-cc-pVTZ level of theory/basis with VPT2 anharmonic correction. Calculated spectra were empirically shifted to recover the experimentally observed positions of the overtone of the out-of-plane H atom, $2\nu_{oop_H}$ transition. The orange peaks are predicted as arising from additional resonances. Figure adapted from Reference 67 with the permission of AIP Publishing.

The lower triangle of the corresponding symmetric Hamiltonian matrix is as follows (90):

$$\mathbf{H} = \begin{pmatrix} 1455.5 & & & & & \\ 3.3 & 1455.5 & & & & \\ 5.1 & 3.3 & 1455.5 & & & \\ 0.8 & 5.1 & 3.3 & 1455.5 & & \\ 5.1 & 0.8 & 5.1 & 3.3 & 1455.5 & \\ 3.3 & 5.1 & 0.8 & 5.1 & 3.3 & 1455.5 \end{pmatrix}. \quad 1.$$

This Hückel-like Hamiltonian describes six degenerate localized CH_2 scissor vibrations that are coupled to each other at the harmonic level. In contrast to valence local modes (91, 92), the localized normal modes are decoupled from all other modes at the harmonic level. As a result, the eigenvalues of this Hamiltonian, which neglect the quadratic couplings proportional to $a_i^\dagger a_j^\dagger + a_i a_j$, correspond to a very good approximation of the results of a normal mode frequency analysis at the B3LYP/6-311++(d,p) level of theory.

The effective Hamiltonian model for the C–H stretches takes a similar form, but this Hamiltonian is more complicated because it includes six axial and six equatorial C–H stretches as well as the overtone and combination states of the CH_2 scissor modes. These modes are included owing to the Fermi mixing that occurs for these vibrations. The effects of anharmonicities and corrections for the use of the DFT level of theory are accounted for by scaling of the diagonal elements of the stretches by 0.960 and the scissors by 0.975 (79). The Fermi coupling, which is localized to the stretch-scissor couplings on individual CH_2 groups, is 22.0 cm^{-1} in this model. Previous work has shown that there are corrections to the cubic contribution at higher orders in perturbation theory (57), so it is expected that this value is less than the values obtained via electronic structure theory. Additional anharmonic contributions are taken from second-order perturbative treatments of model systems and are assumed to be transferable between the scissor and stretch vibrations of all CH_2 and CH_3 groups (79).

Figure 5 shows a result from an investigation into the conformational preferences of pentyl- through decylbenzene (93). These preferences were determined under jet-cooled conditions in the gas phase by combining information from laser-induced fluorescence excitation spectra, FDIR in the alkyl C–H stretch region, and Raman spectra. This particular figure compares the FDIR spectra of the all-*trans* conformer of decylbenzene to the local mode theoretical prediction. The motions that contribute to the spectra are highlighted by dividing the local C–H stretch dipoles into contributions from asymmetric and symmetric CH_2 stretches and a CH_3 stretch contribution and then selectively turning these contributions on and off. The figure also shows those two modes that are linear combinations of the asymmetric modes and that carry the majority of the oscillator strength. Using these comparisons with other conformers in addition to Raman and laser-induced excitation spectra, Hewett et al. (93) were able to identify many conformers, including those that should be characterized as folded structures in which the chain bends back over the phenyl π cloud.

This local mode model was recently extended to include pseudorotation in cyclopentane. This molecule has unusual thermodynamic (94), spectroscopic (95–99), and dynamical properties (97–100) as a result of ring puckering. This puckering leads to a low-frequency internal motion known as pseudorotation (101). This motion is essentially barrierless and can be treated with a particle in a ring Hamiltonian with eigenvalues $E_{rot} = B_\phi \ell^2$, with ℓ taking on integer values and B_ϕ = 2.8 cm^{-1}, a value determined by femtosecond time-resolved Raman rotational coherence spectroscopy (100). The dependence of coupling to C–H stretches and scissors is due to the fact that the pseudorotation leads to the C–H stretches switching from equatorial to axial and back as the pseudorotation angle increases by 2π. By carefully tracking the angular dependence of the

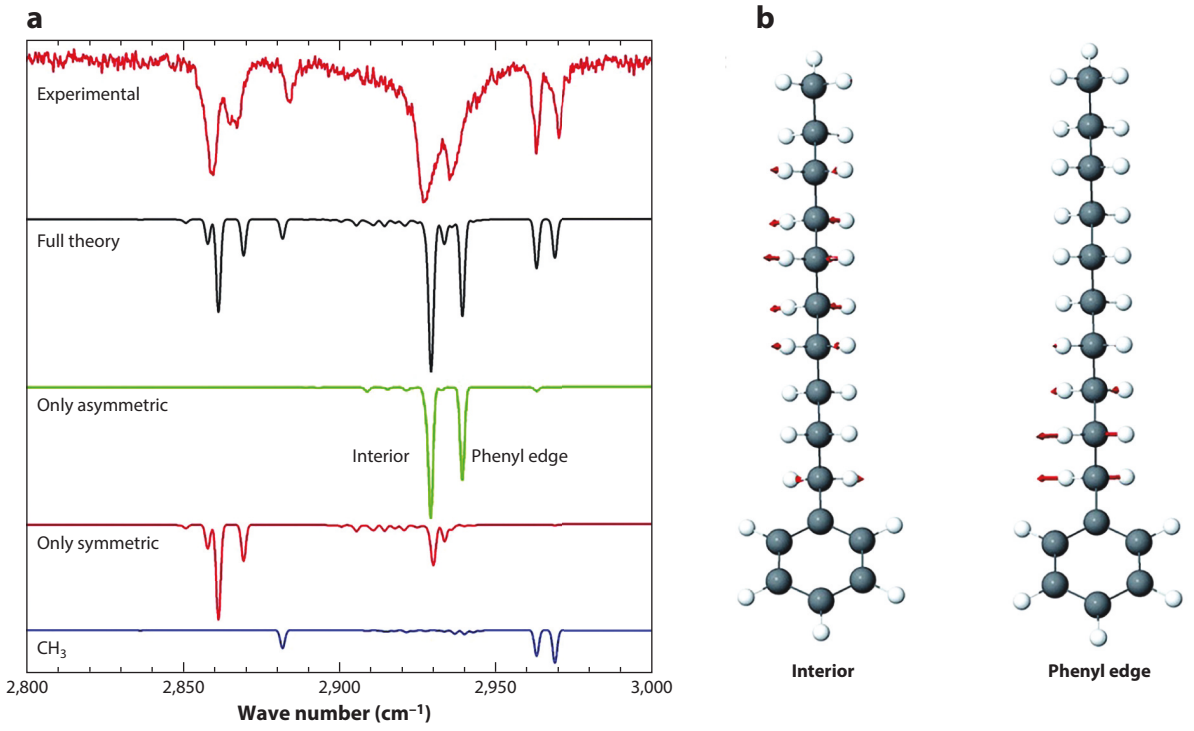

Figure 5

(*a*) Experimental spectrum of the all-*trans* conformer of decylbenzene is compared with the theoretical spectrum and its dipole decomposition. (*b*) The two major delocalized asymmetric modes are displayed as well. Figure adapted from Reference 93 with permission from The Royal Society of Chemistry.

5×5 elements of the local mode scissor Hamiltonian along with the dipoles, the eigenvalues and spectral intensities were calculated in a direct product basis of the one-quantum scissor states and particle in a ring basis function describing the pseudorotation (102).

The resulting prediction is compared to the experimental spectrum in **Figure 6**. In contrast to the above experiments in which the ultracold temperatures of the molecular beam greatly reduce

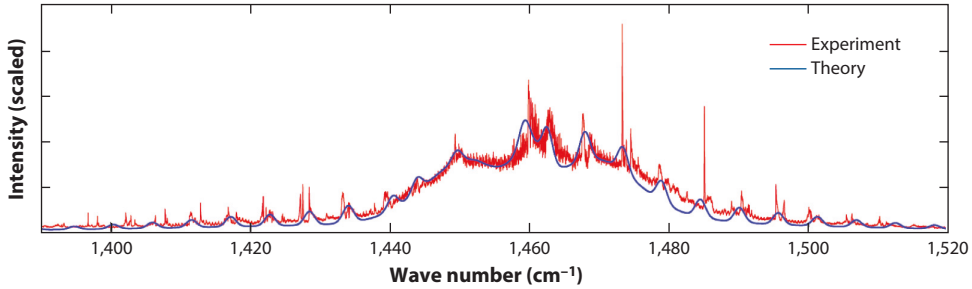

Figure 6

Comparison of experiment and theory. Temperature is −26.1°C. Theoretical intensities are scaled to match experiment. Individual lines are broadened by Gaussian functions $\exp[-(I - I_o)/\sigma^2]$ with $\sigma = 0.25$ cm^{-1}. Figure adapted from Reference 102 with the permission of AIP Publishing.

rotational congestion, these experiments were carried out at a temperature of −26.1°C. As a result there are many initially populated pseudorotation states and both $\Delta\ell = 0$ and ± 1 vibrational transitions are allowed, each being broadened by the rotational profiles expected by the rotational selection rules.

The less than regular spacings observed in **Figure 6** are a result of the coupling between the scissors being modulated by the pseudorotation. The good agreement between theory and experiment provides confidence that DFT force fields are accurately capturing this coupling. The mode mixing is substantially more pronounced in the C–H stretch region, leading to spectra that are qualitatively more complex than those that are usually associated with this spectral regime (103).

5. REDUCED-DIMENSIONAL VARIATIONAL APPROACHES

A second time-honored approach for investigating high-frequency vibrations is to target select molecular vibrations and assume that these vibrations are uncoupled from the remaining degrees of freedom. Recently, the Kuo group has championed the use of this approach and has demonstrated its power in a series of calculations (104–109). As an example, Kuo and colleagues (104, 105) have investigated hydrogen-bond-induced Fermi resonances in N–H···H complexes. Mishra et al. (105) compare theoretical to experimental IR spectra in the N–H stretching regime obtained using IR–UV double-resonance spectroscopic methods (110). The theoretical methods included 3D and 4D normal mode models at the MP2/aug-cc-pVDT level combined with direct product DVR basis sets to set up Hamiltonian matrices whose solutions are determined by direct diagonalization. Three of the degrees of freedom that are included are normal modes associated with the NH_2 stretches and bending; the fourth included a mode that was determined to be in possible Fermi resonance. The essential spectral features were reproduced, but this satisfactory agreement is attributed to the level of theory used to determine the molecular structures.

Using similar theoretical and experimental methods, the IR spectra of neutral dimethylamine $(CH_3)_2NH$ clusters (106) have been investigated in the N–H stretch and C–H stretch methyl stretch regions. The N–H stretches are mostly detuned from the overtone of the bends, so the interesting Fermi couplings are only observed for the C–H stretches. In this study (106), the methyl groups were assumed to be sufficiently decoupled that they could be modeled independently of each other. Furthermore, they were modeled with Hamiltonians that include six localized normal mode degrees of freedom that include three C–H stretches and two bending vibrations and one umbrella vibration. The localization is due to the normal modes being derived from diagonalization of that block of the mass-weighted Cartesian Hessian describing the positions of the four atoms of a methyl group.

Moving away from quartic force fields, generating a highly faithful analytical representation of the discrete data of electronic structure energies for multidimensional systems poses a challenge. Over the past decade, many general fitting approaches have been developed to represent high-dimensional PESs for molecular systems consisting of more than three atoms (111). Common to many of the approaches is representing the potential in the VSCF form, which is a progression of one-body, two-body, and so forth up to M-body terms:

$$V(Q_1, Q_1, \cdots Q_N) = \sum_{i=1}^{N} V_i^{(1)}(Q_i) + \sum_{i=1}^{N}\sum_{j=1}^{N} V_{i,j}^{(2)}(Q_i, Q_j) + \cdots . \qquad 2.$$

The choice of coordinates is flexible, and the value of M can be systematically increased until the desired accuracy is achieved (33, 112–114).

Furthermore, VSCF form simplifies the fit of a full force field to one with at most M dimensions. If the Q_i are also combined with their conjugate momenta to solve the TISE, then the VSCF

form allows for easier evaluation of potential energy matrix elements because all integrations of these elements are less than or equal to M dimensions. The VSCF form blends well with sum of product (SOP) wave functions in tensorial decomposition (115). If one requires a permutationally invariant PES to correctly describe the dynamics of interest, then additional steps should be considered. Such potentials are outside the scope of this review, but they have been reviewed by Qu et al. (12). We note that recent advances of collocation methods (116–118) show promise for moving beyond the VSCF form.

Zhang et al. (106) compared the results of calculations based on potentials in the restricted quartic form used in VPT2 to those based on potentials in the form of Equation 2 with $M = 5$, in which potential-optimized DVR grids were used with five points per degree of freedom. This study also explored hybrid methods in which the 1D and 2D grid points were determined at the CCSD/aug-cc-pVDZ level and 3D to 5D grids were determined at the MP2/aug-cc-pVDZ level. The results, displayed in **Figure 7**, highlight the sensitivity of the spectra to the details of treatment of the PES.

The utility of the localized fragment normal mode approach was further demonstrated in a beautiful study that explored the changes that occur in the N–H stretch spectral region of

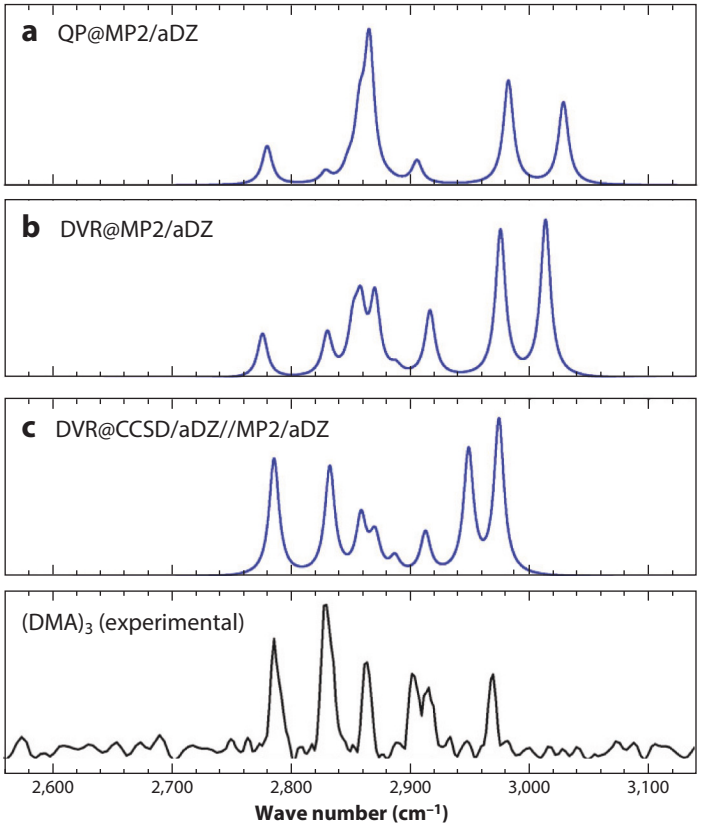

Figure 7

Comparison of theoretical spectra of the C–H stretch region of $(CH_3)_2NH$ (DMA), calculated with (*a*) a quartic potential in restricted quartic form used for VPT2, (*b*) numerical PES using DVR calculated with MP2/aug-cc-pVDZ, and (*c*) the hybrid PES discussed in the text. Experimental data of DMA trimer reported are shown at the bottom for comparison. Figure adapted from Reference 106 with the permission of AIP Publishing.

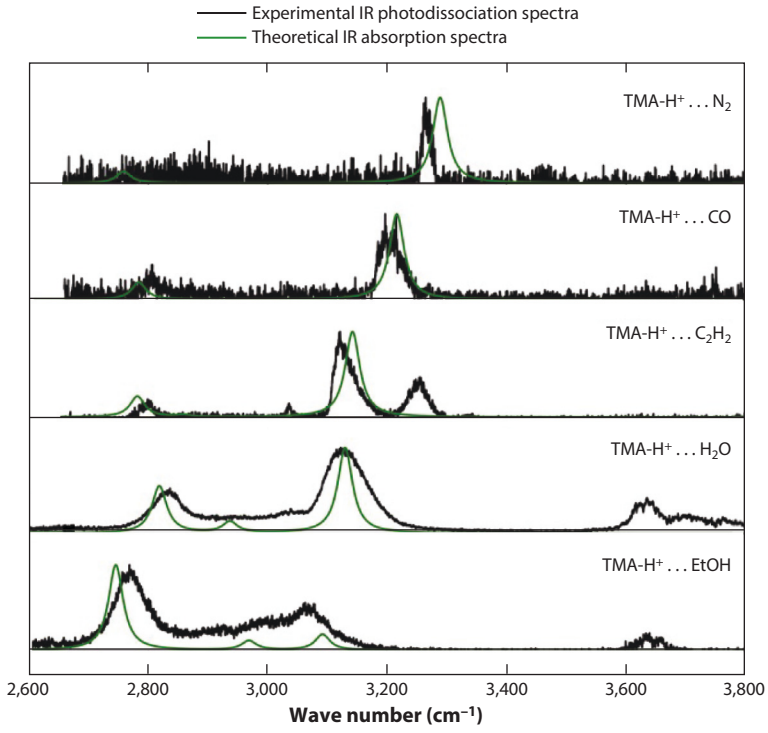

Figure 8

The experimental IR photodissociation spectra (*black*) of TMA-$H^+ \cdots X$ (X = N_2, CO, C_2H_2, H_2O, and EtOH) and theoretical IR absorption spectra (*green*) simulated by the 3D ab initio anharmonic vibrational Hamiltonian at CCSD/aug-cc-pVDZ (119). The series of acceptors moving down the figure is in order of increasing proton affinities, these being 494, 594, 641, 691, and 776 kJ mol^{-1}, all of which are less than the proton affinity of TMA 949 kJ mol^{-1}. Spectra of fully deuterated methyl groups leave positions of peaks unchanged. Figure adapted with permission from Reference 119.

ion–molecule complexes $(CH_3)_3N–H^+ \cdot X$ (TMA-$H^+ \cdots X$) as the proton affinity of X is increased (119). This investigation built on and extends the work of Roscioli et al. (120), who have systematically studied the IR spectra associated with the motions of a proton shared between two closed-shell molecules, [A·H^+ ·B], recognizing the importance of these systems as soft binding motifs in biological processes.

A key result of the Huang et al. (119) work is shown in **Figure 8**, where the spectral series are compared with the theoretical calculations of a localized normal mode fragment model that includes the N–H stretch that is Fermi coupled to the two bending overtones involving the H atom. This compelling study indicates a successively increasing redshift of the N–H stretch as it is tuned past the Fermi-coupled overtones.

The local fragment model of the Kuo group (119, 121) is similar to the local mode monomer (LMM) model of the Bowman group (122–125). In this model, the fragments are the water monomer units. Diagonalization of the Hessian leads to nine degrees of freedom, two of which correspond to the O–H stretching modes and one of which corresponds to the bend. An anharmonic 3D vibrational potential is constructed by considering motions along these normal coordinates, keeping all other coordinates constrained to their equilibrium values. These calculations make use of the many-body water WHBB (Wang–Huang–Braams–Bowman) potential developed by this same group (126). The LMM approach was favorably benchmarked for the

dimer by comparing it with higher-dimensional calculations. This work uses direct diagonalization of Hamiltonian matrices, where the basis functions are obtained in the VSCF approach (127, 128). In the initial work of Wang & Bowman (122), the final spectra predictions are a result of uncoupled monomer modes, but the LMM can be extended to include couplings between the lowest few eigenstates of each monomer (123). The beauty of the LMM is that it can readily be extended to large systems. Recently, Yu & Bowman (125) modeled the vibrational spectroscopy of the three low-lying conformers of the $H_3O^+(H_2O)_{20}$ cluster. All three clusters have similar spectra, and the agreement with experiment is good. The spectral complexity arising in both the theoretical and experimental results makes detailed comparison difficult.

6. VARIATIONAL AND PERTURBATIVE STUDIES OF FORMIC ACID

To illustrate the inherent challenges in the representation of the PES and the solution of the TISE that are faced with medium-sized molecules, we present three distinct treatments of the vibrations of the formic acid molecule. There are extensive spectroscopic data available for this molecule. As such, Suhm and coworkers (129, 130) have championed its use as a benchmark (131) for vibrational models describing coupling pathways. The molecule also has two low-energy conformers shown in **Figure 9** that require potential fitting strategies that extend beyond the typical Taylor series expansion of normal modes.

Before we start comparing approaches, we return to a discussion of the PES and its VSCF form of Equation 2. Quartic representations of potentials remain a popular choice among

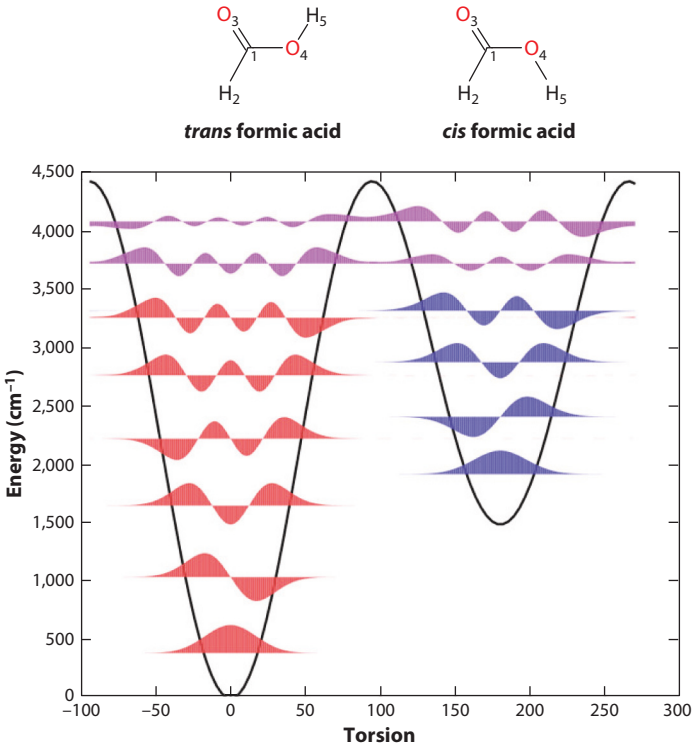

Figure 9

Potential energy curve and torsional states of *trans* and *cis* formic acid. Figure adapted with permission from Reference 132; copyright 2021 American Chemical Society.

research groups that are pushing the limits of our ability to calculate eigenstates of vibrational Hamiltonians. A leading reason is that these representations can be obtained relatively easily from electronic structure calculations. A second reason is that these potentials have an SOP form that is ideal for methods based on tensor decomposition, rapid evaluation matrix-vector products used in iterative methods, and analytical shortcuts that aim to reduce vector storage costs. As an example, Thomas et al. (26) have calculated all the eigenstates of naphthalene up to 1,100 cm^{-1} above the zero-point energy (ZPE) by cleverly reducing the rank of the vectors that need to be stored in the iterative process. An important downside of the quartic potential energy force fields based on normal modes is that they lead to the presence of unphysical conformational regions that require special treatments (133, 134).

For realistic variational calculations, one must move beyond quartic normal mode expansions and consider the more general VSCF form of the potential. The choice of coordinates Q_i to use in a VSCF expansion is an open one. Normal coordinates are most often used because of the excellent zero-order picture they provide and the well-known form of the kinetic energy operator (91). Cheng & Steele (87) realized that by transforming to a set of localized normal modes the VSCF expansions converge more rapidly than those expressed in normal modes without overly increasing the complexity of the kinetic energy operator. Since the early days of force field development (135), it has been recognized that the internal bond-angle extension coordinates provide the best low-order VSCF form (136), and the convergence properties of the localized normal modes follow from this observation. The basic idea is that couplings are localized in space. As an example, let us consider cubic coupling terms. The only important three-body terms are those in which all three valence coordinates are in the same spatial region. Because normal modes can be delocalized over the entire molecule, there are no simple rules as to when one expects these cubic terms to be small.

Richter and colleagues (137, 138) in their adiabatic generation of an adiabatic PES (AGAPES) procedure have pursued the construction of VSCF potentials in which the Q_i in Equation 2 are internal valence coordinates for the reason mentioned above. They have applied the procedure to several systems with excellent success (138–140). The curvilinear form is particularly well suited to instances in which the large-amplitude motion is localized along a single internal coordinate. This is the case for the *cis*/*trans* isomerization of formic acid. An important advance has been the numerical treatment of the complex kinetic energy operators (36, 141, 142) that allows these coordinates to be combined with their conjugate momenta to describe a Hamiltonian. An excellent example of this use can be found in variational treatments of the water dimer (143), in which the authors carefully examined various reduced-dimensional models, such as those described in Section 5, in order to understand the role of couplings in this important hydrogen-bonded system that continues to receive considerable attention (143).

To further improve the accuracy and reduce the number of ab initio points that one must calculate to fit the potential, Richter and colleagues have developed a procedure that determines not only the value of M that should be adopted but also which individual contributions to the M-body term that need to be included. For example, there are many three-body terms, $V^{(3)}_{i,j,k}$, but only some may be important. The procedure they developed answers this question systematically. This selection procedure is based on an iterative procedure in which the contribution of an additional point is judged based on the extent to which its contribution affects the energies contributed from Hamiltonians whose potentials are assumed to follow from the previously calculated $V^{(M-1)}$ terms as well as the current contribution that is being considered. The positions of the coordinates associated with a point to be added are based on a weighted-average interpolation error scheme. As in many surface fitting approaches, the contribution can be fit in a least squares or interpolation procedure using a suitable set of basis functions. For example, for the stretches q_i, Richter

and colleagues (137, 144) expand the potential in terms of Morse functions $[1-\exp(-\alpha q_i)]$. The related interpolation approach of Dawes et al. (2, 3) also has the attractive feature that additional points are chosen automatically based on a given criterion. In these works the points are chosen at the maximal differences between second- and third-order fits in the interpolation.

Richter & Carbonnière (144) applied the AGAPES procedure for formic acid to obtain a full-dimensional formic acid potential, which they fitted to 660 single-point energies at the CCSD(T)-F12a/aVTZ level. The authors report the fit to be accurate up to 13,327 cm^{-1}. This number of points is less than that needed for the full quartic surfaces of the *cis* and *trans* isomers. These authors combined their SOP potential with a kinetic energy operator that can also be written in SOP form, following the work of Gatti & Iung (145) and others. The combination of these two approaches would require large direct product basis sets of individual modes because of the importance of off-diagonal quadratic coupling contributions. However, the SOP form can be combined with the tremendous flexibility of the choices as to how single-particle functions of MCTDH can be defined (40, 43, 146). These choices combined with other enhanced efficiencies such as the block Davidson relaxation scheme allowed for eigenvalue determination over a wide energy range using time-dependent methods.

This study provided energies and eigenfunctions of all the *cis* and *trans* states up to 3,116 cm^{-1} and 4,073 cm^{-1} above the ZPEs, respectively (144). The results were compared with the experimental fundamentals and found to agree within 5 cm^{-1}. The AGAPES interpolation error is based on eigenvalue differences because this is the metric used for the PES fit. The authors report a 2.5 cm^{-1} average error for the vibrational energy levels up to 6,000 cm^{-1} above the ZPE level of about 7,327 cm^{-1}.

Tew & Mizukami (132) chose an alternative method to fit the potential that illustrates a complementary method with enhanced flexibility in fitting at the cost of requiring more ab initio points. Their calculation is performed at a level of theory CCSD(T)(F12*)/cc-pVTZ-F12 comparable to that of Richter & Carbonnière (144), but the form of the potential is very different. To distinguish these potentials, we use the authors' initials and refer to them as the PES-TM and PES-RC surfaces. The PES-TM is not constrained by the VSCF form of Equation 2. Instead it is based on 1D–4D grids of distributed Gaussian basis functions, with the grids being functions of select interatomic distances of atoms. As in the VSCF expansion, the number of required functions rapidly increases as one moves to higher dimensions. Because the Gaussians are functions of the interatomic distances, these potentials can be readily constructed to be invariant to permutation identical nuclei. The huge advantage of the Gaussian basis is that it allows one to fit a much greater variety of shapes of potential energy landscapes.

There are two key additions to the fitting procedure that lead to its success. First, the fit potential is the difference between the ab initio potential and a potential written as a sum of 1D Morse oscillators that in turn are functions of internuclear distances. The parameters of the Morse functions are chosen so that their inclusion leads to the asymptotic form of the fit potential being amenable to the Gaussian fitting. We have found that it is important to avoid fitting potentials with Gaussians whenever the grid includes regions of rapidly increasing potentials, such as those describing the inner repulsive walls, and their approach minimizes this problem. An attractive feature of their algorithm is that the widths and positions of the Gaussians are preselected, based on the choice of internal distance grids, which leads to a surface that is linearly dependent on the unknown Gaussian expansion coefficients. The second attractive feature is the use of the LASSO least squares method (147). Here, the coefficients of the Gaussian basis functions are determined subject to a penalty that is proportional to the sum of the absolute values of the coefficients. Ideally the LASSO fits include only those functions that are most needed in the data fitting. In principle,

this procedure avoids overfitting of data and leads to a reduction in the fluctuations in the fits that often arise from the overfitting.

Tew & Mizukami (132) fit 17,076 single-point energies using 90% for the training set and 10% for the control set. In comparing to the ab initio data in the energy range 0 cm^{-1}–15,000 cm^{-1}, they report root-mean-square deviations of 8 cm^{-1} in the training set and 18 cm^{-1} for the control set. This range includes an accurate treatment of the large-amplitude torsion that is needed for properly describing the 4,500 cm^{-1} barrier to isomerization from the *trans* to the *cis* conformer. The large number of data points required to obtain this accuracy is a result of using fitting basis functions whose linear combinations are able to describe a wide variety of shapes as opposed to functions such as Morse functions that are tailor made for specific bonding types.

To solve the nuclear TISE, Tew & Mizukami used their program DYNAMOL (37) combined with a Hamiltonian in the Hougen–Bunker–Johns (148) form. This Hamiltonian, when generalized as an internal coordinate path Hamiltonian (ICPH), is written in terms of a large-amplitude curvilinear coordinate describing the torsion and $3N - 7$ normal coordinates that are orthogonal to the torsion and the vectors describing the rotation and overall translation of the molecule. Here, N is the number of atoms. The ICPH is designed to minimize couplings among all the modes by correctly treating curvature as necessary while retaining the advantages of the reduced coupling of the normal modes where possible. The basis set used in the calculation is based off of the appropriate boundary conditions; they use trigonometric functions for the torsion and harmonic oscillator basis functions for the remaining degrees of freedom. The potential matrix elements are calculated via quadrature. It is assumed that it is sufficient to restrict couplings up to those of M-body terms, where M is varied from 3 to 5 to test the validity of this approximation. The convergence of their variational vibrational configuration interaction (VCI) calculation is tested by successively increasing the total number of quanta allowed in the configuration interaction calculations as well as the value of M.

Nejad & Sibert (149) benchmarked second- and higher-order perturbation theory using the above potentials and the corresponding variational results. These workers used a numerical version of canonical Van Vleck perturbation theory (CVPT) (55, 57, 141). The numerical approach allows one to use local or normal modes as well as curvilinear or rectilinear modes. The input is a Hamiltonian written in terms of harmonic raising and lowering operators. They chose raising and lowering operators of the curvilinear normal modes. They used the above two potentials by expanding them in a Taylor series. The internal coordinate potential includes up to four-body terms. These contributions include Taylor series expansion terms up to eighth, sixth, sixth, and fourth for the one- to four-body terms, respectively. Simons–Parr–Finlan coordinates were used for the stretches to improve the convergence properties (150). The exact kinetic energy operator (151) is a function of the **G**-matrix elements. These elements are expanded through sixth order in the internal coordinates with the exception of four-body terms, which are expanded through fourth order. The potential-like contribution to the kinetic energy (151) is expanded through fourth order. The spirit of the CVPT is to perturbatively transform away the off-resonant couplings and then treat the remaining couplings between any possible near-degenerate states via diagonalization of relatively small matrices.

The convergence of the perturbative results are shown in **Figure 10*a*** for the *cis* isomer. The differences in nth order CVPT energies $E(n)$ are plotted as a function of $E(6)$ energies. The difference $E(6) - E(4)$ is a measure of the uncertainty of the $E(6)$ results. The matrices used for describing the state mixing in each conformer consisted of a few hundred states.

The CVPT energy difference $E(6) - E(2)$ is a gauge of the accuracy of VPT2 energies, as these latter energies are closely related to CVPT energies $E(2)$. For PES-TM, a comparison for fundamentals and states with two quanta of excitation yields mean absolute deviations (maximum

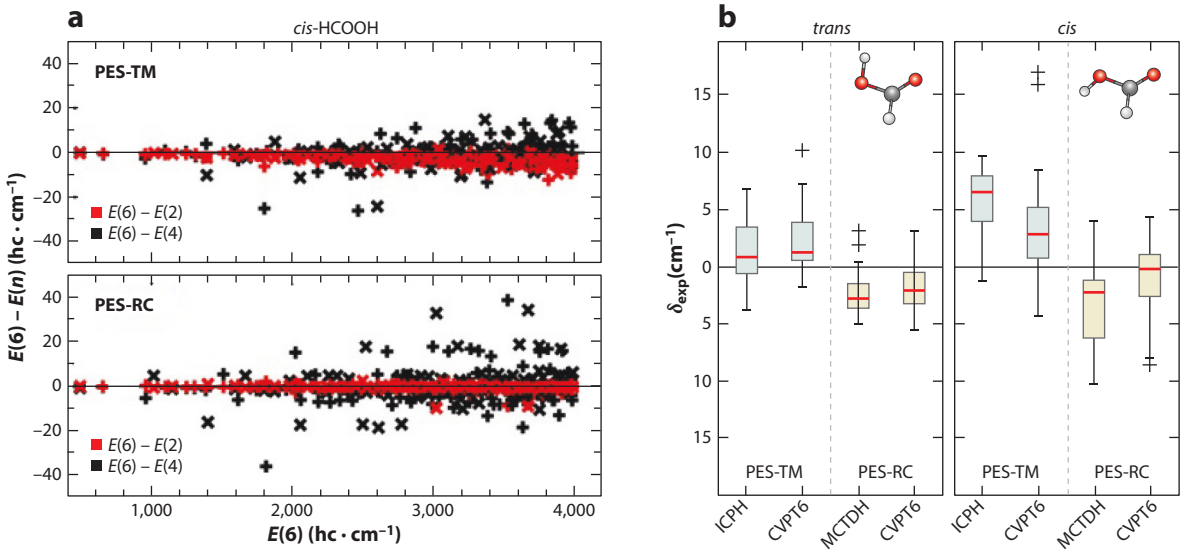

Figure 10

(*a*) CVPT energy differences $E(6) - E(n)$ plotted as a function of $E(6)$ for *cis*-HCOOH vibrational states, where n is the order of the perturbation theory. States of a' and a'' symmetry are marked as crosses and exes, respectively. Only states best described as having a maximum sum of four quanta of excitation are shown. (*b*) Deviation between experimental and computed formic acid fundamental wave numbers ($\delta_{exp} = \tilde{\nu}_{calc} - \tilde{\nu}_{exp}$). Data for all four H/D isotopologs are aggregated for *cis* and *trans* formic acid with 16 and 42 data points, respectively. Plot compares CVPT (149) with ICPH (132) and MCTDH (144) for both conformers. These 42 points comprise 35 *trans* fundamentals and their resonance partners that include the torsional overtone. For the ICPH model (132), 10 and 8 data points are used, respectively, as the O–H stretch fundamental of *cis* is not reported, and deuterated data are not available. Each box extends from the lower quartile to the upper quartile of the data, and whiskers extend out to twice the interquartile range. Outliers are marked as crosses, and each box is bisected by a line indicating the median. Figure adapted from Reference 149 with the permission of AIP Publishing.

absolute deviations) below 1(3) cm^{-1} and 2(6) cm^{-1}, respectively. The limitations of VPT2 are revealed beyond two quanta, where the maximum absolute deviations compared to sixth order CVPT amount to 19 cm^{-1} and 16 cm^{-1} for three- and four-quanta states, respectively.

The deviations between experiment and anharmonic fundamental calculations employing both PESs are visualized in **Figure 10*b***. The comparisons include fundamentals of all deuterated isotopologs. The $E(6)$ results for *trans*-HCOOH compare favorably with ICPH (132) and MCTDH (144) reference data on their respective surfaces; eigenvalues agree to within 2 cm^{-1}. Comparison for *cis*-HCOOH indicates that the ICPH eigenvalues are not fully converged. In addition, the $E(6)$ result with PES-TM yields a *cis*-O–H stretch fundamental transition energy that is 16 cm^{-1} wave numbers greater than experiment. Nejad & Sibert (149) argue that this disparity results from a shortcoming of the surface, based on the size of $E(6) - E(4)$.

The three methods described above are sufficiently accurate and detailed to aid in spectral assignments. Using the results of these calculations Nejad & Sibert (149) assigned 11 new vibrational band centers to the *trans*-HCOOH database and 53 for its three deuterated isotopologs. Profiting from the synergy between accurate calculations and symmetry information from depolarized Raman spectra, they reassigned eight literature IR bands up to 4,000 cm^{-1} above the ZPE.

As the results of **Figure 10** show, the weakest link between theory and experiment remains the quality of the PES. Many of the deviations are systematic, and one can take these deviations into consideration as one maps out the coupling pathways and experimentally observed mode mixing in order to study vibrations at the level of eigenstate resolution. Nejad et al. (130) discuss

the couplings as they relate to the C–H and O–H stretches of formic acid. Both these vibrations show evidence of state mixing. As an example, for the *trans*-O–H stretch the sixth-order CVPT calculation predicts transitions at 3,576 cm^{-1} and 3,568 cm^{-1} for the PES-TM and PES-RC surfaces, respectively. These values are within 1 cm^{-1} of the corresponding ICPH (132) and MCTDH (144) calculations. The experimental results, in contrast, indicate three closely spaced lines, with the most intense band at 3,570.5 cm^{-1}. The detailed discussion of the possible background states involved in this triad (149) illustrates how the increasing densities of states lead to many possible candidates that, in turn, complicate the analysis of this band. The assignments of states quickly become insurmountable as the densities of states increase and mode mixing becomes more universal. As this occurs, one must begin to consider lower-resolution spectra and their intensity patterns as a way of highlighting short-term energy flow processes and the couplings that induce them. Although it has not been stated, these were the approaches being employed for the larger systems that were previously discussed in this review.

Before concluding, we note that the major advantages of the VCI (132) and MCTDH approaches (144) are that they can be used to investigate the large-amplitude motion. The CVPT results require separate calculations for each of the isomers and, as currently formulated, fail in the description of highly excited torsional states, especially states with more than six quanta of torsional excitation (see **Figure 9**) in the *trans* conformer.

7. SUMMARY

In this article, we have described a range of theoretical research that supports the synergistic collaboration between theoreticians and experimentalists working to interpret and utilize the wealth of structural and dynamical information encoded in the vibrational spectra of molecules. This is a broad and rapidly advancing field, and we have chosen to cover a select yet wide variety of techniques for calculating spectra. Both our choice and our discussion highlight the many common underlying strategies that are used as well as draw attention to how specific approaches can be optimized for the challenges that specific coupling scenarios present.

DISCLOSURE STATEMENT

The author is not aware of any affiliations, memberships, funding, or financial holdings that might be perceived as affecting the objectivity of this review.

ACKNOWLEDGMENTS

E.L.S. gratefully acknowledges support from the National Science Foundation via grant CHE-1900095.

LITERATURE CITED

1. Sumpter B, Getino C, Noid D. 1992. A neural network approach to the study of internal energy-flow in molecular-systems. *J. Chem. Phys.* 97:293–306
2. Dawes R, Thompson DL, Guo Y, Wagner AF, Minkoff M. 2007. Interpolating moving least-squares methods for fitting potential energy surfaces: computing high-density potential energy surface data from low-density ab initio data points. *J. Chem. Phys.* 126(18):184108
3. Dawes R, Thompson DL, Wagner AF, Minkoff M. 2008. Interpolating moving least-squares methods for fitting potential energy surfaces: a strategy for efficient automatic data point placement in high dimensions. *J. Chem. Phys.* 128(8):084107

4. Braams BJ, Bowman JM. 2009. Permutationally invariant potential energy surfaces in high dimensionality. *Int. Rev. Phys. Chem.* 28:577–606
5. Evenhuis CR, Collins MA. 2009. Locally optimized coordinates in modified Shepard interpolation. *J. Phys. Chem. A* 113(16):3979–87
6. Frankcombe TJ, Collins MA, Zhang DH. 2012. Modified Shepard interpolation of gas-surface potential energy surfaces with strict plane group symmetry and translational periodicity. *J. Chem. Phys.* 137(14):144701
7. Behler J. 2011. Neural network potential-energy surfaces in chemistry: a tool for large-scale simulations. *Phys. Chem. Chem. Phys.* 13:17930
8. Jiang B, Guo H. 2013. Permutation invariant polynomial neural network approach to fitting potential energy surfaces. *J. Chem. Phys.* 139:054112
9. Jiang B, Li J, Guo H. 2016. Potential energy surfaces from high fidelity fitting of *ab initio* points: the permutation invariant polynomial - neural network approach. *Int. Rev. Phys. Chem.* 35:479–506
10. Behler J. 2015. Constructing high-dimensional neural network potentials: a tutorial review. *Int. J. Quantum Chem.* 115:1032–50
11. Nandi A, Qu C, Bowman JM. 2019. Using gradients in permutationally invariant polynomial potential fitting: a demonstration for CH_4 using as few as 100 configurations. *J. Chem. Theory Comput.* 15:2826–35
12. Qu C, Yu Q, Bowman JM. 2018. Permutationally invariant potential energy surfaces. *Annu. Rev. Phys. Chem.* 69:151–75
13. Unke OT, Koner D, Patra S, Käser S, Meuwly M. 2020. High-dimensional potential energy surfaces for molecular simulations: from empiricism to machine learning. *Mach. Learn. Sci. Tech.* 1:013001
14. Colbert DT, Miller WH. 1992. A novel discrete variable representation for quantum mechanical reactive scattering via the *S*-matrix Kohn method. *J. Chem. Phys.* 96(3):1982–91
15. Cullum JK, Willoughby RA. 1985. *Lanczos Algorithms for Large Symmetric Eigenvalues Computations*. Boston: Birkhäuser
16. Alacid M, Leforestier C. 1998. Direct calculation of long time correlation functions using an optical potential. *Int. J. Quantum Chem.* 68(5):317–28
17. Wang XG, Carrington T. 2003. A contracted basis-Lanczos calculation of vibrational levels of methane: solving the Schrödinger equation in nine dimensions. *J. Chem. Phys.* 119:101–17
18. Stanton JF. 2009. On the vibronic level structure in the NO_3 radical: II. Adiabatic calculation of the infrared spectrum. *Mol. Phys.* 107(8–12):1059–75
19. Haupa KA, Johnson BA, Sibert EL, Lee YP. 2017. Infrared absorption spectra of partially deuterated methoxy radicals CH_2DO and CHD_2O isolated in solid *para*-hydrogen. *J. Chem. Phys.* 147(15):154305
20. Mohankumar N, Carrington T. 2019. A comparison of methods for determining the time step when propagating with the Lanczos algorithm. *Mathematics* 7(11):1109
21. Sibert EL, Blodgett KN, Zwier TS. 2021. Spectroscopic manifestations of indirect vibrational state mixing: novel anharmonic effects on a prereactive H atom transfer surface. *J. Phys. Chem. A* 125(33):7318–30
22. Ribeiro F, Iung C, Leforestier C. 2002. Calculation of highly excited vibrational levels: a prediagonalized Davidson scheme. *Chem. Phys. Lett.* 362(3–4):199–204
23. Garnier R. 2019. Dual vibration configuration interaction (DVCI). An efficient factorization of molecular Hamiltonian for high performance infrared spectrum computation. *Comp. Phys. Comm.* 234:263–77
24. Thomas PS, Carrington T Jr. 2015. Using nested contractions and a hierarchical tensor format to compute vibrational spectra of molecules with seven atoms. *J. Phys. Chem. A* 119(52):13074–91
25. Thomas PS, Carrington T Jr. 2017. An intertwined method for making low-rank, sum-of-product basis functions that makes it possible to compute vibrational spectra of molecules with more than 10 atoms. *J. Chem. Phys.* 146(20):204110
26. Thomas PS, Carrington T Jr., Agarwal J, Schaefer HF. 2018. Using an iterative eigensolver and intertwined rank reduction to compute vibrational spectra of molecules with more than a dozen atoms: uracil and naphthalene. *J. Chem. Phys.* 149(6):064108
27. Rakhuba M, Oseledets I. 2016. Calculating vibrational spectra of molecules using tensor train decomposition. *J. Chem. Phys.* 145(12):124101

28. Madsen NK, Godtliebsen IH, Christiansen O. 2017. Efficient algorithms for solving the non-linear vibrational coupled-cluster equations using full and decomposed tensors. *J. Chem. Phys.* 146(13):134110
29. Soley MB, Bergold P, Batista VS. 2021. Iterative power algorithm for global optimization with quantics tensor trains. *J. Chem. Theory Comp.* 17(6):3280–91
30. Soley MB, Bergold P, Gorodetsky AA, Batista VS. 2022. Functional tensor-train Chebyshev method for multidimensional quantum dynamics simulations. *J. Chem. Theory Comp.* 18:25–36
31. Beylkin G, Mohlenkamp M. 2005. Algorithms for numerical analysis in high dimensions. *SIAM J. Sci. Comp.* 26(6):2133–59
32. Yurchenko SN, Thiel W, Jensen P. 2007. Theoretical rovibrational energies (trove): a robust numerical approach to the calculation of rovibrational energies for polyatomic molecules. *J. Mol. Spec.* 245(2):126–40
33. Carter S, Bowman JM, Handy NC. 1998. Extensions and tests of 'multimodes': a code to obtain accurate vibration/rotation energies of many-mode molecules. *Theor. Chem. Acc.* 100(1–4):191–98
34. Bowman JM, Carter S, Huang X. 2003. Multimode: a code to calculate rovibrational energies of polyatomic molecules. *Int. Rev. Phys. Chem.* 22(3):533–49
35. Fabri C, Matyus E, Csaszar AG. 2011. Rotating full- and reduced-dimensional quantum chemical models of molecules. *J. Chem. Phys.* 134(7):074105
36. Csaszar AG, Fabri C, Szidarovszky T, Matyus E, Furtenbacher T, Czako G. 2012. The fourth age of quantum chemistry: molecules in motion. *Phys. Chem. Chem. Phys.* 14(3):1085–106
37. Mizukami W, Tew DP. 2013. A second-order multi-reference perturbation method for molecular vibrations. *J. Chem. Phys.* 139(19):194108
38. Sibaev M, Crittenden DL. 2016. PyVCI: a flexible open-source code for calculating accurate molecular infrared spectra. *Comp. Phys. Comm.* 203:290–97
39. Sibaev M, Crittenden DL. 2016. Balancing accuracy and efficiency in selecting vibrational configuration interaction basis states using vibrational perturbation theory. *J. Chem. Phys.* 145(6):064106
40. Beck M, Jackle A, Worth G, Meyer H. 2000. The multiconfiguration time-dependent Hartree (MCTDH) method: a highly efficient algorithm for propagating wavepackets. *Phys. Rep.* 324:1–105
41. Manthe U. 2008. A multilayer multiconfigurational time-dependent Hartree approach for quantum dynamics on general potential energy surfaces. *J. Chem. Phys.* 128(16):164116
42. Manthe U. 2009. Layered discrete variable representations and their application within the multiconfigurational time-dependent Hartree approach. *J. Chem. Phys.* 130(5):054109
43. Meyer HD. 2012. Studying molecular quantum dynamics with the multiconfiguration time-dependent Hartree method. *Wiley Interdiscip. Rev. Comp. Mol. Sci.* 2(2):351–74
44. Carney J, Zwier T. 2000. The infrared and ultraviolet spectra of individual conformational isomers of biomolecules: tryptamine. *J. Phys. Chem. A* 104(38):8677–88
45. Dian BC, Longarte A, Mercier S, Evans DA, Wales DJ, Zwier TS. 2002. The infrared and ultraviolet spectra of single conformations of methyl-capped dipeptides: N-acetyl tryptophan amide and N-acetyl tryptophan methyl amide. *J. Chem. Phys.* 117(23):10688–702
46. Masson A, Kamrath MZ, Perez MAS, Glover MS, Rothlisberger U, et al. 2015. Infrared spectroscopy of mobility-selected H^+-Gly-Pro-Gly-Gly (GPGG). *J. Am. Soc. Mass Spectrom.* 26(9):1444–54
47. Garand E, Kamrath MZ, Jordan PA, Wolk AB, Leavitt CM, et al. 2012. Determination of noncovalent docking by infrared spectroscopy of cold gas-phase complexes. *Science* 335(6069):694–98
48. Boyarkin OV. 2018. Cold ion spectroscopy for structural identifications of biomolecules. *Int. Rev. Phys. Chem.* 37(3–4):559–606
49. Burke NL, DeBlase AF, Redwine JG, Hopkins JR, McLuckey SA, Zwier TS. 2016. Gas-phase folding of a prototypical protonated pentapeptide: spectroscopic evidence for formation of a charge-stabilized beta-hairpin. *J. Am. Chem. Soc.* 138(8):2849–57
50. DeBlase AF, Dziekonski ET, Hopkins JR, Burke NL, Sheng H, et al. 2016. Alkali cation chelation in cold beta-o-4 tetralignol complexes. *J. Phys. Chem. A* 120(36):7152–66
51. DeBlase AF, Harrilal CP, Lawler JT, Burke NL, McLuckey SA, Zwiere TS. 2017. Conformation-specific infrared and ultraviolet spectroscopy of cold $[YAPAA+H]^+$ and $[YGPAA+H]^+$ ions: a stereochemical "twist" on the β-hairpin turn. *J. Am. Chem. Soc.* 139(15):5481–93

52. Andersson M, Uvdal P. 2005. New scale factors for harmonic vibrational frequencies using the B3LYP density functional method with the triple-ζ basis set 6-311+g(d,p). *J. Phys. Chem. A* 109(12):2937–41
53. Fischer KC, Sherman SL, Garand E. 2020. Competition between solvation and intramolecular hydrogen-bonding in microsolvated protonated glycine and β-alanine. *J. Phys. Chem. A* 124(8):1593–602
54. Lawler JT, Harrilal CP, DeBlase AF, Sibert EL, McLuckey SA, Zwier TS. 2022. Single-conformation spectroscopy of cold, protonated ^{D}PG-containing peptides: switching β-turn types and formation of a sequential type II/II′ double β-turn. *Phys. Chem. Chem. Phys.* 24(4):2095–109
55. Nielsen HH. 1945. The vibration-rotation energies of polyatomic molecules part II. Accidental degeneracies. *Phys. Rev.* 68(7–8):181–91
56. Herman RC, Shaffer WH. 1948. The calculation of perturbation energies in vibrating rotating polyatomic molecules. *J. Chem. Phys.* 16(5):453–65
57. McCoy AB, Sibert EL. 1990. Perturbative approaches to highly excited molecular vibrations of H_2O, D_2O and HDO. *J. Chem. Phys.* 92:1893–901
58. Kauppi E, Halonen L. 1995. 5-dimensional local mode-Fermi resonance model for overtone spectra of ammonia. *J. Chem. Phys.* 103(16):6861–72
59. Mackeprang K, Hanninen V, Halonen L, Kjaergaard HG. 2015. The effect of large amplitude motions on the vibrational intensities in hydrogen bonded complexes. *J. Chem. Phys.* 142(9):094304
60. Puzzarini C, Biczysko M, Barone V. 2011. Accurate anharmonic vibrational frequencies for uracil: the performance of composite schemes and hybrid CC/DFT model. *J. Chem. Theory Comp.* 7(11):3702–10
61. Maslen PE, Handy NC, Amos RD, Jayatilaka D. 1992. Higher analytic derivatives. IV. Anharmonic effects in the benzene spectrum. *J. Chem. Phys.* 97(6):4233–54
62. Roy TK, Carrington JT, Gerber RB. 2014. Approximate first-principles anharmonic calculations of polyatomic spectra using MP2 and B3LYP potentials: comparisons with experiment. *J. Phys. Chem. A* 118(33, SI):6730–39
63. Roy TK. 2022. Performance of vibrational self-consistent field theory for accurate potential energy surfaces: fundamentals, excited states, and intensities. *J. Phys. Chem. A* 126(4):608–622
64. Maltseva E, Petrignani A, Candian A, Mackie CJ, Huang X, et al. 2015. High-resolution IR absorption spectroscopy of polycyclic aromatic hydrocarbons: the realm of anharmonicity. *Astrophys. J.* 814:23
65. Mackie CJ, Candian A, Huang X, Maltseva E, Petrignani A, et al. 2016. The anharmonic quartic force field infrared spectra of five non-linear polycyclic aromatic hydrocarbons: benz[a]anthracene, chrysene, phenanthrene, pyrene, and triphenylene. *J. Chem. Phys.* 145(8):084313
66. Mackie CJ, Candian A, Huang X, Maltseva E, Petrignani A, et al. 2018. The anharmonic quartic force field infrared spectra of hydrogenated and methylated PAHs. *Phys. Chem. Chem. Phys.* 20(2):1189–97
67. Stropoli SJ, Khuu T, Boyer MA, Karimova VN, Gavin-Hanner CF, et al. 2022. Electronic and mechanical anharmonicities in the vibrational spectra of the H-bonded, cryogenically cooled $X^- \cdot HOCl$ (X = Cl, Br, I) complexes: characterization of the strong anionic H-bond to an acidic OH group. *J. Chem. Phys.* 156(17):174303
68. Stropoli SJ, Khuu T, Messinger JP, Karimova VN, Boyer MA, et al. 2022. Preparation and characterization of the halogen-bonding motif in the isolated $Cl^- \cdot IOH$ complex with cryogenic ion vibrational spectroscopy. *J. Phys. Chem. Lett.* 13(12):2750–56
69. Boyer MA, McCoy AB. 2022. A flexible approach to vibrational perturbation theory using sparse matrix methods. *J. Chem. Phys.* 156(5):054107
70. Franke PR, Tabor DP, Moradi CP, Douberly GE, Agarwal J, et al. 2016. Infrared laser spectroscopy of the *n*-propyl and *i*-propyl radicals: stretch-bend Fermi coupling in the alkyl CH stretch region. *J. Chem. Phys.* 145(22):224304
71. Franke PR, Stanton JF, Douberly GE. 2021. How to VPT2: accurate and intuitive simulations of CH stretching infrared spectra using VPT2+K with large effective Hamiltonian resonance treatments. *J. Phys. Chem. A* 125(6):1301–24
72. Barnes GL, Kellman ME. 2011. Detailed analysis of polyad-breaking spectroscopic Hamiltonians for multiple minima with above barrier motion: isomerization in HO_2. *J. Chem. Phys.* 134(7):074108
73. Mackie CJ, Candian A, Huang X, Maltseva E, Petrignani A, et al. 2015. The anharmonic quartic force field infrared spectra of three polycyclic aromatic hydrocarbons: naphthalene, anthracene, and tetracene. *J. Chem. Phys.* 143(22):224314

74. Kim HL, Kulp TJ, McDonald JD. 1987. Infrared fluorescence study on the threshold of intramolecular vibrational-state mixing. *J. Chem. Phys.* 87(8):4376–82
75. Almlöf J, Taylor PR. 1987. General contraction of Gaussian basis sets. I. Atomic natural orbitals for first- and second-row atoms. *J. Chem. Phys.* 86(7):4070–77
76. Buchanan EG, Dean JC, Zwier TS, Sibert EL. 2013. Towards a first-principles model of Fermi resonance in the alkyl CH stretch region: application to 1,2-diphenylethane and 2,2,2-paracyclophane. *J. Chem. Phys.* 138(6):064308
77. Buchanan EG, Sibert EL, Zwier TS. 2013. Ground state conformational preferences and CH stretch-bend coupling in a model alkoxy chain: 1,2-diphenoxyethane. *J. Phys. Chem. A* 117(13):2800–11
78. Kidwell NM, Mehta-Hurt DN, Korn JA, Sibert EL, Zwier TS. 2014. Ground and excited state infrared spectroscopy of jet-cooled radicals: exploring the photophysics of trihydronaphthyl and inden-2-ylmethyl. *J. Chem. Phys.* 140(21):214302
79. Tabor DP, Hewett DM, Bocklitz S, Korn JA, Tomaine AJ, et al. 2016. Anharmonic modeling of the conformation-specific IR spectra of ethyl, *n*-propyl, and *n*-butylbenzene. *J. Chem. Phys.* 144(22):224310
80. Blodgett KN, Sun D, Fischer JL, Sibert EL, Zwier TS. 2019. Vibronic spectroscopy of methyl anthranilate and its water complex: hydrogen atom dislocation in the excited state. *Phys. Chem. Chem. Phys.* 21:21355–69
81. Tabor DP, Kusaka R, Walsh PS, Sibert EL, Zwier TS. 2015. Isomer-specific spectroscopy of benzene-$(H_2O)_n$, $n = 6, 7$: benzene's role in reshaping water's three-dimensional networks. *J. Phys. Chem. Lett.* 6(10):1989–95
82. Sibert EL. 2019. Modeling vibrational anharmonicity in infrared spectra of high frequency vibrations of polyatomic molecules. *J. Chem. Phys.* 150(9):090901
83. Bernath PF, Bittner DM, Sibert EL. 2019. Isobutane infrared bands: partial rotational assignments, ab initio calculations, and local mode analysis. *J. Phys. Chem. A* 123(29):6185–93
84. Jacob CR, Reiher M. 2009. Localizing normal modes in large molecules. *J. Chem. Phys.* 130(8):84106
85. Weymuth T, Jacob CR, Reiher M. 2010. A local-mode model for understanding the dependence of the extended amide III vibrations on protein secondary structure. *J. Phys. Chem. B* 114(32):10649–60
86. Sibert EL. 2013. Dressed local mode Hamiltonians for CH stretch vibrations. *Mol. Phys.* 111(14–15):2093–99
87. Cheng X, Steele RP. 2014. Efficient anharmonic vibrational spectroscopy for large molecules using local-mode coordinates. *J. Chem. Phys.* 141(10):104105
88. Cheng X, Talbot JJ, Steele RP. 2016. Tuning vibrational mode localization with frequency windowing. *J. Chem. Phys.* 145(12):124112
89. Zimmerman PM, Smereka P. 2016. Optimizing vibrational coordinates to modulate intermode coupling. *J. Chem. Theory Comp.* 12(4):1883–91
90. Bernath PF, Sibert EL. 2020. Cyclohexane vibrations: high-resolution spectra and anharmonic local mode calculations. *J. Phys. Chem. A* 124(48):9991–10000
91. Wilson EB, Decius JC, Cross PC. 1955. *Molecular Vibrations*. New York: McGraw-Hill
92. Halonen L. 1998. Local mode vibrations in polyatomic molecules. In *Advances in Chemical Physics*, Vol. 104, ed. I Prigogine, SA Rice, pp. 41–179. New York: John Wiley & Sons, Ltd.
93. Hewett DM, Bocklitz S, Tabor DP, Sibert EL, Suhm MA, Zwier TS. 2017. Identifying the first folded alkylbenzene via ultraviolet, infrared, and Raman spectroscopy of pentylbenzene through decylbenzene. *Chem. Sci.* 8(8):5305–18
94. Kilpatrick JE, Pitzer KS, Spitzer R. 1947. The thermodynamics and molecular structure of cyclopentane. *J. Am. Chem. Soc.* 69(10):2483–88
95. Chao TH, Laane J. 1978. Vibrational studies of cyclopentane: effect of 10-fold barrier to pseudorotation. *J. Mol. Spec.* 70(3):357–60
96. Bauman LE, Laane J. 1988. Pseudorotation of cyclopentane and its deuterated derivatives. *J. Phys. Chem.* 92(5):1040–51
97. MacPhail RA, Variyar JE. 1989. Pseudorotation dynamics in liquid cyclopentane by Raman spectroscopy. *Chem. Phys. Lett.* 161(3):239–44
98. Variyar JE, MacPhail RA. 1992. Pseudorotation and the Raman CH stretching spectrum of gaseous cyclopentane-D_9: local modes in a floppy molecule. *J. Phys. Chem.* 96(2):576–84

99. Pan X, MacPhail R. 1993. A Raman-study of cyclopentane-d_9 pseudorotation dynamics as a function of pressure. *Chem. Phys. Lett.* 212(1–2):64–70
100. Kowalewski P, Frey HM, Infanger D, Leutwyler S. 2015. Probing the structure, pseudorotation, and radial vibrations of cyclopentane by femtosecond rotational Raman coherence spectroscopy. *J. Phys. Chem. A* 119(45):11215–25
101. Strauss HL. 1983. Pseudorotation: a large amplitude molecular motion. *Annu. Rev. Phys. Chem.* 34:301–28
102. Sibert EL, Bernath PF. 2022. A local mode study of ring puckering effects in the infrared spectra of cyclopentane. *J. Chem. Phys.* 156:214305
103. Sax AF. 2008. On pseudorotation. *Chem. Phys.* 349(1–3):9–31
104. Ho KL, Lee LY, Katada M, Fujii A, Kuo JL. 2016. An *ab initio* anharmonic approach to study vibrational spectra of small ammonia clusters. *Phys. Chem. Chem. Phys.* 18(44):30498–506
105. Mishra S, Kuo JL, Patwari GN. 2018. Hydrogen bond induced enhancement of Fermi resonances in N–H . . . N hydrogen bonded complexes of anilines. *Phys. Chem. Chem. Phys.* 20(33):21557–66
106. Zhang B, Huang QR, Jiang S, Chen LW, Hsu PJ, et al. 2019. Infrared spectra of neutral dimethylamine clusters: an infrared-vacuum ultraviolet spectroscopic and anharmonic vibrational calculation study. *J. Chem. Phys.* 150(6):064317
107. Lin C, Huang Q, Hayashi M, Kuo J. 2021. An *ab initio* anharmonic approach to IR, Raman and SFG spectra of the solvated methylammonium ion. *Phys. Chem. Chem. Phys.* 23(45):25736–47
108. Lin C, Huang Q, Li Y, Nguyen H, Kuo J, Fujii A. 2021. Anharmonic coupling revealed by the vibrational spectra of solvated protonated methanol: Fermi resonance, combination bands, and isotope effect. *J. Phys. Chem. A* 125(9):1910–18
109. Feng J, Lee Y, Witek HA, Hsu P, Kuo J, Ebata T. 2021. Structures of pyridine–water clusters studied with infrared–vacuum ultraviolet spectroscopy. *J. Phys. Chem. A* 125(34, SI):7489–501
110. Zhang B, Kong X, Jiang S, Zhao Z, Yang D, et al. 2017. Infrared-vacuum ultraviolet spectroscopic and theoretical study of neutral methylamine dimer. *J. Phys. Chem. A* 121(38):7176–82
111. Christiansen O. 2012. Selected new developments in vibrational structure theory: potential construction and vibrational wave function calculations. *Phys. Chem. Chem. Phys.* 14(19):6672–87
112. Jung J, Gerber R. 1996. Vibrational wave functions and energy levels of large anharmonic clusters: a vibrational SCF study of Ar_{13}. *J. Chem. Phys.* 105(24):10682–90
113. Chaban G, Jung J, Gerber R. 1999. *Ab initio* calculation of anharmonic vibrational states of polyatomic systems: electronic structure combined with vibrational self-consistent field. *J. Chem. Phys* 111(5):1823–29
114. Heindel JP, Xantheas SS. 2020. The many-body expansion for aqueous systems revisited: I. Water–water interactions. *J. Chem. Theory Comp.* 16(11):6843–55
115. Kallullathil SD, Carrington T Jr. 2021. Computing vibrational energy levels by solving linear equations using a tensor method with an imposed rank. *J. Chem. Phys.* 155(23):234105
116. Simmons J, Carrington T Jr. 2021. Using collocation and solutions for a sum-of-product potential to compute vibrational energy levels for general potentials. *Chem. Phys. Lett.* 781:138967
117. Wodraszka R, Carrington T Jr. 2021. A rectangular collocation multi-configuration time-dependent Hartree (MCTDH) approach with time-independent points for calculations on general potential energy surfaces. *J. Chem. Phys.* 154(11):114107
118. Flynn SW, Mandelshtam VA. 2021. Molecular spectra calculations using an optimized quasi-regular Gaussian basis and the collocation method. *J. Chem. Theory Comp.* 17(11):7169–77
119. Huang QR, Shishido R, Lin CK, Tsai CW, Tan JA, et al. 2021. Strong Fermi resonance associated with proton motions revealed by vibrational spectra of asymmetric proton-bound dimers. *Angew. Chem. Int. Ed.* 60(4):1936–41
120. Roscioli JR, McCunn LR, Johnson MA. 2007. Quantum structure of the intermolecular proton bond. *Science* 316(5822):249–54
121. Kuo J. 2021. Disentangling the complex vibrational spectra of hydrogen-bonded clusters of 2-pyridone with *ab initio* structural search and anharmonic analysis. *J. Phys. Chem. A* 125(20):4306–12
122. Wang Y, Bowman JM. 2011. *Ab initio* potential and dipole moment surfaces for water. II. Local-monomer calculations of the infrared spectra of water clusters. *J. Chem. Phys.* 134(15):154510

123. Wang Y, Bowman JM. 2012. Coupled-monomers in molecular assemblies: theory and application to the water tetramer, pentamer, and ring hexamer. *J. Chem. Phys.* 136(14):144113
124. Liu H, Wang Y, Bowman JM. 2014. Local-monomer calculations of the intramolecular IR spectra of the cage and prism isomers of $HOD(D_2O)_5$ and HOD and D_2O ice I_h. *J. Phys. Chem. B* 118(49):14124–31
125. Yu Q, Bowman JM. 2020. Tracking hydronium/water stretches in magic $H_3O^+(H_2O)_{20}$ clusters through high-level quantum VSCF/VCI calculations. *J. Phys. Chem. A* 124(6, SI):1167–75
126. Wang Y, Huang X, Shepler BC, Braams BJ, Bowman JM. 2011. Flexible, *ab initio* potential, and dipole moment surfaces for water. I. Tests and applications for clusters up to the 22-mer. *J. Chem. Phys.* 134(9):094509
127. Bowman JM. 1978. Self-consistent field energies and wavefunctions for coupled oscillators. *J. Chem. Phys.* 68(2):608–10
128. Gerber R, Ratner M. 1979. A semiclassical self-consistent field (SC-SCF) approximation for eigenvalues of coupled-vibration systems. *Chem. Phys. Lett.* 68:195–98
129. Meyer KAE, Suhm MA. 2019. Stretching of *cis*-formic acid: warm-up and cool-down as molecular work-out. *Chem. Sci.* 10(25):6285–94
130. Nejad A, Suhm MA, Meyer KAE. 2020. Increasing the weights in the molecular work-out of *cis*- and *trans*-formic acid: extension of the vibrational database via deuteration. *J. Chem. Phys.* 22(44):25492–501
131. Mata RA, Suhm MA. 2017. Benchmarking quantum chemical methods: Are we heading in the right direction? *Angew. Chem. Int. Ed.* 56(37, SI):11011–18
132. Tew DP, Mizukami W. 2016. Ab initio vibrational spectroscopy of *cis*- and *trans*-formic acid from a global potential energy surface. *J. Phys. Chem. A* 120(49):9815–28
133. Pandey A, Poirier B. 2020. Plumbing potentials for molecules with up to tens of atoms: how to find saddle points and fix leaky holes. *J. Phys. Chem. Lett.* 11(15):6468–74
134. Pandey A, Poirier B. 2020. An algorithm to find (and plug) "holes" in multi-dimensional surfaces. *J. Chem. Phys.* 152(21):214102
135. Hoy A, Mills I, Strey G. 1972. Anharmonic force constant calculations. *Mol. Phys.* 24(6):1265–90
136. Richter F, Carbonniere P, Pouchan C. 2014. Toward linear scaling: locality of potential energy surface coupling in valence coordinates. *Int. J. Quantum Chem.* 114(20, SI):1401–11
137. Richter F, Carbonniere P, Dargelos A, Pouchan C. 2012. An adaptive potential energy surface generation method using curvilinear valence coordinates. *J. Chem. Phys.* 136(22):224105
138. Richter F, Carbonnière P. 2022. Vibrational treatment of hydroxylamine in valence coordinates. *J. Chem. Phys.* 156(8):084306
139. Richter F, Thaunay F, Lauvergnat D, Carbonnière P. 2015. Anharmonic vibrational treatment exclusively in coordinates: the case of formamide curvilinear valence. *J. Phys. Chem. A* 119(48):11719–28
140. Aerts A, Carbonnière P, Richter F, Brown A. 2020. Vibrational states of deuterated *trans*- and *cis*-formic acid: DCOOH, HCOOD, and DCOOD. *J. Chem. Phys.* 152(2):024305
141. McCoy AB, Burleigh DC, Sibert EL. 1991. Rotation-vibration interactions in highly excited states of SO_2 and H_2CO. *J. Chem. Phys.* 95(10):7449–65
142. Luckhaus D. 2000. 6D vibrational quantum dynamics: generalized coordinate discrete variable representation and (a)diabatic contraction. *J. Chem. Phys.* 113(4):1329–47
143. Vogt E, Simkó I, Császár AG, Kjaergaard HG. 2022. Reduced-dimensional vibrational models of the water dimer. *J. Chem. Phys.* 156(16):164304
144. Richter F, Carbonnière P. 2018. Vibrational treatment of the formic acid double minimum case in valence coordinates. *J. Chem. Phys.* 148(6):064303
145. Gatti F, Iung C. 2009. Exact and constrained kinetic energy operators for polyatomic molecules: the polyspherical approach. *Phys. Rep.* 484(1–2):1–69
146. Bowman JM, Carrington T Jr., Meyer HD. 2008. Variational quantum approaches for computing vibrational energies of polyatomic molecules. *Mol. Phys.* 106(16–18):2145–82
147. Tibshirani R. 1996. Regression shrinkage and selection via the lasso. *J. R. Stat. Soc. Ser. B Meth.* 58:267–88
148. Hougen J, Bunker P, Johns J. 1970. Vibration-rotation problem in triatomic molecules allowing for a large-amplitude bending vibration. *J. Mol. Spec.* 34:136–72

149. Nejad A, Sibert EL. 2021. The Raman jet spectrum of *trans*-formic acid and its deuterated isotopologs: combining theory and experiment to extend the vibrational database. *J. Chem. Phys.* 154(6):064301
150. Simons G, Parr RG, Finlan JM. 1973. New alternative to the Dunham potential for diatomic molecules. *J. Chem. Phys.* 59(6):3229–34
151. Pickett HM. 1972. Vibration–rotation interactions and the choice of rotating axes for polyatomic molecules. *J. Chem. Phys.* 56(4):1715–23

Annual Review of Physical Chemistry
Volume 74, 2023

Contents

Errata

An online log of corrections to *Annual Review of Physical Chemistry* articles may be found at http://www.annualreviews.org/errata/physchem